Secondary Stabilization Reactions and Proton-Coupled Electron Transport in Photosystem II Investigated by Electroluminescence and Fluorescence Spectroscopy †

ARTICLE *in* BIOCHEMISTRY · MAY 2001

Impact Factor: 3.02 · DOI: 10.1021/bi002824z · Source: PubMed

3 AUTHORS, INCLUDING:

Hans J. van Gorkom
Leiden University
100 PUBLICATIONS **4,746** CITATIONS

SEE PROFILE

Secondary Stabilization Reactions and Proton-Coupled Electron Transport in Photosystem II Investigated by Electroluminescence and Fluorescence Spectroscopy†

Rik de Wijn, Thijs Schrama,‡ and Hans J. van Gorkom*

Department of Biophysics, Leiden University, P.O. Box 9504, 2300 RA Leiden, The Netherlands

Received December 13, 2000

ABSTRACT: The oxidized primary electron donor in photosystem II, P_{680}^+, is reduced in several phases, extending over 4 orders of magnitude in time. Especially the slower phases may reflect the back-pressure exerted by water oxidation and provide information on the reactions involved. The kinetics of secondary electron-transfer reactions in the microseconds time range after charge separation were investigated in oxygen-evolving thylakoids suspended in H_2O or D_2O. Flash-induced changes of chlorophyll fluorescence yield and electric field-induced recombination luminescence were decomposed into contributions from oxidation states S_0, S_1, S_2, and S_3 of the oxygen-evolving complex and interpreted in terms of stabilization kinetics of the initial charge-separated state $S_jY_ZP_{680}^+Q_A^-Q_B$. In approximately 10% of the centers, only charge recombination took place. Otherwise, no static heterogeneity was involved in the microsecond reduction of P_{680}^+ by Y_Z (stabilization) or Q_A^- (recombination). The recombination component in active centers occurs mainly upon charge separation in S_3, and, in the presence of D_2O, in S_2 as well and is tentatively attributed to the presence of $Y_Z^{ox}S_{j-1}$ in equilibrium with Y_ZS_j. A 20−30 μs stabilization occurs in all S-states, but to different extents. Possible mechanisms for this component are discussed. D_2O was found to decrease: (i) the rate of the reaction $Y_Z^{ox}S_1$ to Y_ZS_2, (ii) the equilibrium constant between $P680^+Y_ZS_2$ and $P_{680}Y_Z^{ox}S_2$, (iii) the rate of the slow phase of P_{680}^+ reduction for the $S_3 \rightarrow S_0$ transition, and (iv) the rate of electron transfer from Q_A^- to Q_B /Q_B^-. The increased 'miss probability' in D_2O is due to (iii).

The PS II[1] reaction center is unique because it uses water as a source of electrons. To do so it needs to couple the one-electron process of charge separation to the four-electron process of water oxidation. On the donor side of the reaction center (RC), the charge separation is stabilized by electron transfer from a redox-active tyrosine (Y_Z) to P_{680}^+. The oxidized tyrosine, Y_Z^{ox}, is in turn reduced by a four-manganese cluster which is the active site for water oxidation. This complex can store 4 oxidizing equiv by cycling through five so-called S-states, S_0-S_4, the subscript indicating the number of equivalents stored. After oxidation of Y_Z in the S_3 state, the complex spontaneously decays to S_0, producing molecular oxygen by the oxidation of two water molecules [for a review of PS II function, see ref (*1*)].

Following formation of $P_{680}^+Q_A^-$, reduction of P_{680}^+ by Y_Z (stabilization) occurs in competition with recombination (reduction of P_{680}^+ by Q_A^-). The stabilization reaction occurs with a time constant of 20−300 ns (depending on S-state) (*2*), which is much faster than the recombination reaction (time constant 100 μs, or slower), so dissipation of charge separation energy is effectively minimized. However, there are many reports in the literature concerning P_{680}^+ reduction kinetics in the microseconds time range. This is well-known to occur in PS II RCs that have been inactivated by destruction of the manganese cluster. Here, P_{680}^+ reduction by Y_Z occurs with a time constant of 15 μs at pH 6.5; this rate is dependent on pH and H_2O/D_2O exchange (*3*−*6*). When in these centers a second charge separation occurs while Y_Z is still oxidized, the charge separation cannot be stabilized, and $P_{680}^+Q_A^-$ is lost by charge recombination with a time constant in the 100−200 μs range (*3*, *4*, *7*). Microsecond phases connected to P_{680}^+ reduction have also been observed in active, oxygen-evolving centers. Delayed and prompt fluorescence measurements by Zankel (*8*, *9*) showed the existence of 35 μs (and faster) and 200 μs kinetic phases that exhibited period 4 oscillations typical for active S-state cycles. These phases have been equated with reduction of P_{680}^+ (*10*−*14*), e.g., either as a stabilization or as a recombination (possibly involving an electron acceptor different from Q_A), and under the usual conditions of measurement, such phases form a minor part of the total extent of P_{680}^+ reduction kinetics. However, under physiological conditions, the pH at the PS II donor side may well be lowered to pH 5−5.5 due to the proton gradient formed by steady-state electron transfer. At this pH, the extent of

†This research was supported by the section Chemical Sciences of the Netherlands Organization for Scientific Research (NWO-CW).

* Corresponding author. Telephone: ++31 71 5275969. Fax: ++31 71 5275819. E-mail: vanGorkom@Biophys.LeidenUniv.nl.

‡ Current address: Swammerdam Institute for Life Science, University of Amsterdam, Kruislaan 316, 1098 SM Amsterdam, The Netherlands.

[1] Abbreviations: DCMU, 3-(3′,4′-dichlorophenyl)-1,1-dimethylurea; EL, electroluminescence; P_{680}, special chlorophyll, primary electron donor; PS II, photosystem II; Q_A, primary quinone acceptor; Q_B, secondary quinone acceptor; RC, reaction center; Tricine, *N*-[tris-(hydroxylmethyl)methyl]glycine; Tris, tris(hydroxymethyl)aminomethane; Y_Z, tyrosine-Z (Tyr-D1−161), secondary electron donor.

10.1021/bi002824z CCC: $20.00
Published on Web 04/21/2001

microsecond P_{680}^+ reduction was found to be considerably higher (*12*), so the slow kinetic phases of P_{680}^+ reduction may be physiologically relevant.

Interest in the microsecond phases of P_{680}^+ reduction was recently revived in connection with speculations on the function of Y_Z. One model proposes that Y_Z is actively involved in water oxidation by acting as a hydrogen atom abstractor from manganese-bound water (*15*, *16*). Dissociation of the phenolic proton of Y_Z that accompanies its oxidation (*17*) constitutes the first step in the proposed mechanism for ejection of water protons into the lumen, and should occur on each S-state transition. This model conflicts with measurements of local electrochromism that indicate that the positive charge remains in the vicinity of Y_Z (*18*) and the stoichiometry of H^+ release is 1:0:1:2 for the successive S-state transitions (*19*).

Y_Z must be deprotonated for its oxidation by P_{680}^+, and a histidine residue (D1-His190) is proposed to be the acceptor for this proton (*20*). If the state Y_Z^{ox}-His190(H^+) is energetically unfavorable, stabilization would occur by proton transfer to secondary acceptors (*21*). If this tyrosine proton is replaced by hydrogen atom transfer from substrate water, H_2O/D_2O exchange would likely produce significant effects on P_{680}^+ reduction; it has been observed that the slower phases of this reduction are markedly different in D_2O (*22*−*24*). From a study of flash number dependence, it was concluded that D_2O enhanced $P_{680}^+Q_A^-$ recombination in S_2 and S_3 (*22*). This was tentatively attributed to a retardation of the "35 μs" reduction of P_{680}^+, but the cross-correlation between the values of fit parameters did not allow an unbiased decomposition of the kinetics.

To what extent the slow components in P_{680}^+ reduction reflect recombination rather than stabilization, and static or dynamic PS II heterogeneity rather than a stepwise relaxation in all centers, is presently not clear. Yet such information is essential to evaluate the implications of the slow P_{680}^+ reduction phases for our understanding of water oxidation.

We have investigated these questions by electroluminescence (EL) measurements which explore the electrogenicity of photosynthetic charge separation to obtain information on the electron-transfer reactions involved (*25*). By exposing a suspension of osmotically swollen chloroplasts (blebs) to an external electric field, electric potentials of up to 1 V can be generated over the thylakoid membrane. When the polarity of the induced electric field is such that it opposes the transmembrane charge separation, recombination reactions in the photosynthetic reaction centers are strongly enhanced. This causes an increase in the population of the singlet excited state of P_{680} and therefore an increased probability of loss of the excitation by fluorescence emission: electroluminescence (EL). Vos et al. (*26*) used EL to investigate stabilization reactions on the donor side of PS II on the submilliseconds to seconds time scale. At their time resolution, they could barely resolve a large component that might be related to "35 μs" P_{680}^+ reduction. In this paper, we present EL induced within the first millisecond after a flash. Using lower electric field strength to eliminate PSI contributions (*27*), and a better time resolution, we have distinguished EL from $P_{680}^+Q_A^-$ recombination from that emitted by more stable states ($Y_Z^{ox}Q_A^-$ in particular) by their different kinetics. Fluorescence yield measurements were used to distinguish stabilization from recombination reactions, and the effect of D_2O on each kinetic parameter in each S-state was analyzed, using a Monte Carlo fit simulation procedure to extract quantitative conclusions from the fits despite cross-correlations between fit parameters.

MATERIALS AND METHODS

Thylakoids were isolated from fresh spinach leaves (*28*) and stored until use in small portions in liquid nitrogen in a buffer containing 25 mM Tricine (pH 7.8), 0.4 M sucrose, 15 mM NaCl, and 5 mM $MgCl_2$. Osmotically swollen thylakoid membranes (blebs) were prepared shortly before measurement by diluting the chloroplast suspension (2 mg/mL Chl) 400-fold in either D_2O or H_2O containing 1 mM 3-(*N*-morpholino)propanesulfonic acid (MOPS) and 1 mM $CaCl_2$ (pH 6.6 in H_2O). To obtain an equivalent pD in D_2O, the solution was adjusted to a pH-meter readout of 6.2 (*29*). Before starting the measurements, blebs were dark-adapted in a sample reservoir for 15 min after dilution. All experiments were carried out at room temperature (20 °C).

The measurement cuvette consisted of two ~1 × 1 cm platinum electrodes spaced at 2 mm by a piece of rectangular glass tube surrounding the sample. Samples could be loaded and refreshed from the sample reservoir via two small slits directly under and above one of the electrodes by opening an automated valve. Emitted light was collected by placing the sample in a focus of an ellipsoidal mirror and detected by a photomultiplier tube (EMI 9816A) through KV 550 and RG 630 cutoff filters and an 686 nm interference filter. Saturation of the photomultiplier tube by the exciting laser flashes was avoided by employing an electronic gate (*30*) to shut it off during flashes.

Electroluminescence kinetics were measured by exposing the sample to a 180 μs electric field pulse (0.9 kV/cm) generated by a home-built pulsed high voltage supply at an adjustable time after a series of 1−12 saturating flashes from a frequency-doubled Nd:YAG laser (fwhm 10 ns, 10 Hz). The photomultiplier signal was amplified (bandwidth >1 MHz) and recorded by an ADC operating at a sample frequency of 2 MHz that was interfaced to a PC for data averaging and storage. A fresh dark-adapted sample was used for each measurement. A luminescent background was subtracted so that the electroluminescence was taken to be the photomultiplier signal with electric field pulse minus the signal without the pulse. The contribution of PS I to the EL signal was insignificant at electric field strengths of 1 kV/cm in this preparation (data not shown).

Flash-induced fluorescence changes were measured under the same conditions as the EL measurements. Fluorescence was excited by three blue LED's (MARL, 470 nm) pulsed by a 1 A, 2 μs pulse from a current driver at an adjustable time after the flash series. A Corning CS4-96 optical filter filtered the measuring light. The photomultiplier signal just before, during, and after the LED pulse was sampled transiently at 20 MHz, and the fluorescence yield at the set delay time was calculated by the measuring software using time integration over the duration of the LED pulse and a linear baseline correction. Each data point is the average of three measurements.

Least-squares fitting was performed using the routine e04jaf of the NAG toolbox for Matlab. This routine employs a quasi-Newton method to minimize a general nonlinear

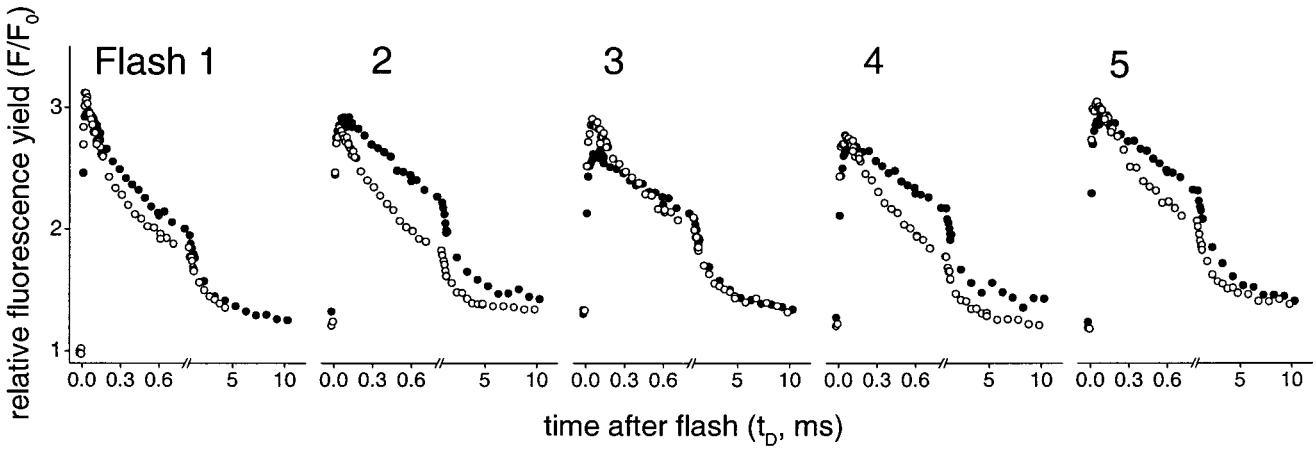

FIGURE 1: Fluorescence yield changes induced by the last of 1−5 flashes in dark-adapted blebs suspended in H_2O (open circles) or D_2O (solid circles). F_0 is taken as the fluorescence level before the first flash. The first points of each trace were taken shortly before the last flash; the first point after was at $t_D = 10$ ms. Note the change in scaling at $t_D = 0.8$ ms.

function and allows bounds to be imposed on the parameters. Confidence intervals of estimated parameters were obtained by a Monte Carlo method (*31*). The method consists of first obtaining the most likely parameters by an ordinary least-squares fit of the real data. This fit is used to generate a large number of synthetic datasets by adding random noise with the same distribution as found in the original data. All synthetic datasets are then fitted in the same way as the original data to produce a distribution of values for each fit parameter. These distributions represent the confidence intervals including cross-correlations between the parameters.

RESULTS

Flash-Induced Fluorescence Yield Changes. Since the chlorophyll fluorescence yield of PS II is much lower when either Q_A or P_{680} is in the oxidized state than when both are reduced, the flash-induced fluorescence change provides a measure of electron transfer by these cofactors (*32*). Dark-adapted blebs were illuminated with a series of saturating laser flashes spaced at 100 ms, and the fluorescence excited by a 2 μs pulse of measuring light was detected at a variable delay time, t_D, after the last flash (Figure 1). The data are normalized to the fluorescence yield in the dark-adapted state (F_0). In the presence of DCMU, which blocks electron transfer beyond Q_A^-, the maximum fluorescence yield observed after two or more flashes was 3.7 in both H_2O and D_2O (not shown). In the absence of DCMU, and also after a single saturating flash in its presence, this value is not reached because of a significant probability that charge recombination takes place before Y_Z reduces P_{680}^+, an efficient nonphotochemical excitation trap. The small fluorescence yield increase indicated by the first few points after the unresolved initial rise suggests that in some PS II centers the reduction of P_{680}^+ by Y_Z takes tens of microseconds, instead of 20−300 ns. Fluorescence quenching by carotenoid triplets in the antenna, which have a lifetime of 3 μs (*33*), may explain why the first point after the flash is lower, but cannot account for the later increase. The highest fluorescence yield is observed after about 50 μs. In the 10 ms time range measured, the subsequent decrease is dominated by a submillisecond phase attributed to electron transfer to Q_B or Q_B^-, and by a phase of a few milliseconds that we attribute to centers in which this reaction is delayed because the Q_B binding site was empty at the moment of the flash. At later times, the fluorescence yield decays much slower, and even after 100 ms, just before the next flash, it is still about 20% above F_0.

The amplitude and kinetics of the fluorescence yield changes are weakly but characteristically dependent on the number of flashes fired. The initial decay after one flash is clearly faster than after two flashes, which is usually explained by a slower electron transfer from Q_A^- to Q_B^- than to Q_B. However, obvious binary oscillations with flash number as in refs (*34*, *35*) were not observed, and the results shown here are more similar to those of Putrenko et al. (*36*). In D_2O (solid circles), the fluorescence yield decreases more slowly, in agreement with (*37*). This effect seems more pronounced on even-numbered flashes, i.e., on electron transfer from Q_A^- to Q_B^-.

The measurements of Figure 1 show that blebs exhibit all the well-known PS II fluorescence yield changes on this time scale, including the rise attributed to a slow phase in P_{680}^+ reduction. This suggests that the charge pair $P_{680}^+Q_A^-$ should be present in detectable amounts during the first 50 μs after a flash, which should allow a characterization of kinetics by EL measurements with excellent signal-to-noise ratio.

Electroluminescence Measurements. EL measurements were carried out under the same conditions as the fluorescence yield measurements, but instead of the 2 μs fluorescence excitation light pulse, a 180 μs electric field pulse of 900 V/cm was applied at the desired delay time after the flash series. Figure 2 shows typical traces measured at $t_D =$ 10 and 150 μs. The signals observed in the absence of the field pulse have been subtracted. The EL intensity and its decay kinetics during the field pulse show a pronounced dependence on the number of flashes fired and on the delay between the last flash and the pulse. At $t_D = 10$ μs, the EL traces appear to contain a rapidly decaying component that is missing in the traces measured at $t_D = 150$ μs. In H_2O, this component is about equally large after two and three flashes whereas the slower component that dominates the signal toward the end of the pulse when it is applied at 10 ms and throughout the pulse at $t_D = 150$ μs is much smaller after two flashes. This is not the case in D_2O; suspension of the sample in D_2O appears to enhance specifically the amplitude of the slow component after two flashes, appar-

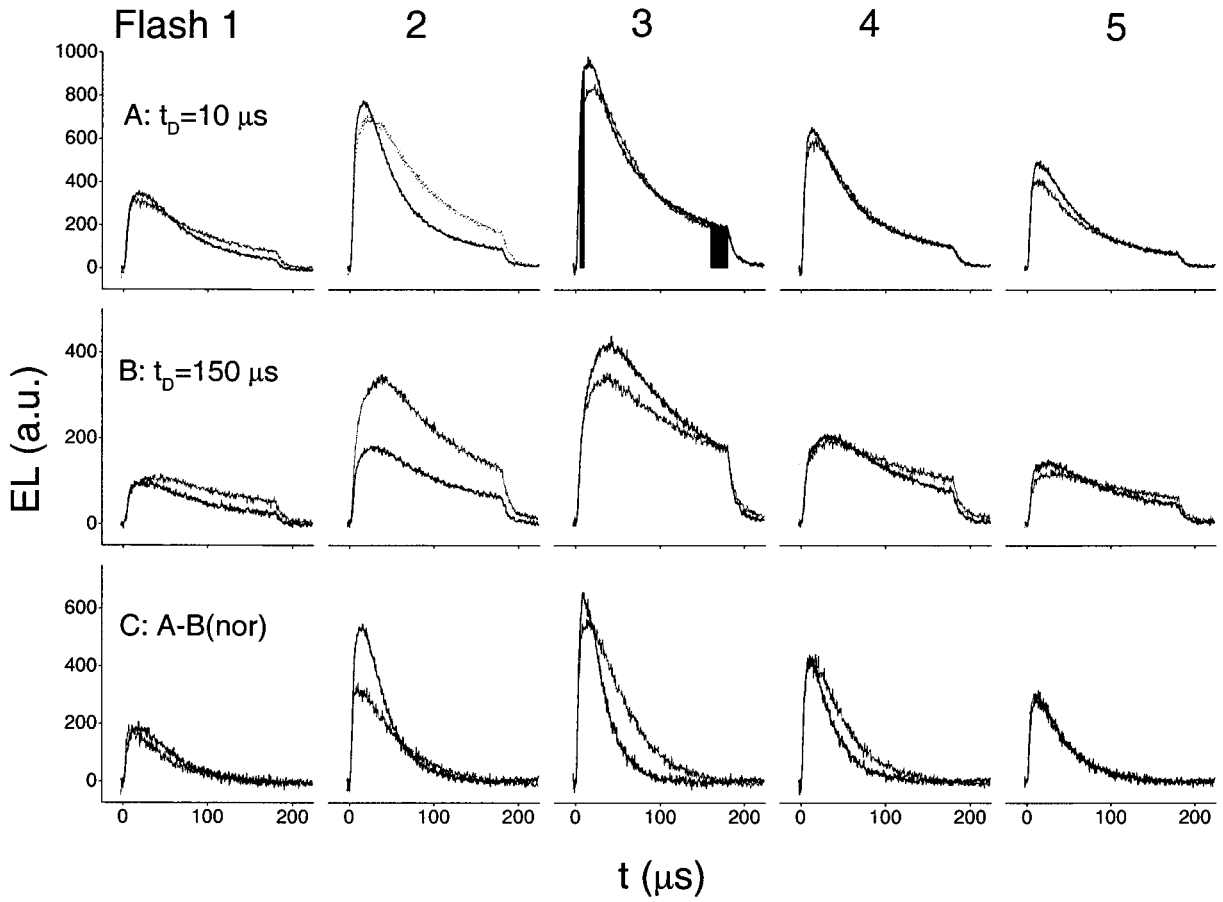

FIGURE 2: EL transients generated by a 180 μs, 0.9 kV/cm electric field pulse switched on at $t = 0$ at two different delay times (t_D) after the last of 1−5 flashes; upper panels (A), $t_D = 10$ μs; middle panels (B), $t_D = 150$ μs. In the bottom panels (C), the kinetics of the fast component are approximated by subtracting the kinetics in (B) from the kinetics in (A) after normalization on the last points during the pulse. Note the difference in vertical scaling between the upper, middle, and lower panels. Solid lines, blebs suspended in H_2O; dotted lines, in D_2O. The black areas under the trace after the third flash (H_2O) indicate the integration ranges of 5−10 and 160−180 μs after the onset of the electric field pulse, referred to in the text as early and late EL, respectively.

ently at the expense of the fast component. The EL traces measured after $t_D = 150$ ms also indicate that D_2O slows down the kinetics of the slow component during the pulse, except after two flashes. The kinetics of the fast component may be visualized in a first approximation by the traces in the bottom panels in Figure 2 which show the difference between the signals at $t_D = 10$ μs and $t_D = 150$ μs after they were normalized at the end of the pulse. The main difference between the fast component in H_2O and D_2O is that in D_2O the amplitude of this component is lower after the second flash and its kinetics are somewhat slower after the third flash.

Either kinetic component can be selected, at every t_D, by taking the signal amplitude at the beginning or at the end of the pulse. To select the early emission, the EL signal was integrated from 5 to 10 μs after the onset of the pulse; for the late emission, an integration interval from 160 to 180 μs was used. The black areas in Figure 2 (featured for flash 3 in the top panel) indicate the values thus obtained for the early and late emission.

EL Precursor Decay Kinetics. Figure 3 shows the amplitudes of the early (solid circles) and late (open circles) EL as a function of the delay time t_D between the flash and the onset of the electric field pulse. In H_2O or D_2O, the state that gives rise to the early EL disappears more rapidly than the state causing late EL. The precursor of the early EL decays in two distinct phases at the time scale of our measurement. The fast phase occurs in tens of microseconds; its amplitude varies strongly with the number of flashes given before the electric field is applied. After an intermediate phase of about 100−200 μs, some EL remains that could be due to the precursor of the late EL. Both the amplitude and the decrease of the late EL as a function of t_D show a pronounced flash number dependence, clearly different from that of the fast phase of early EL. In some cases, especially after the third flash in H_2O, the precursor of the late EL even shows an initial increase. The marked effect of D_2O on the amplitude of late EL after two flashes was already seen in Figure 2. Its effect on the initial rise after two or three flashes may be related to its effect on the decay of the precursor of early EL.

These results show that at short times after a flash most of the early EL comes from recombination of a different charge pair, which largely disappears within 150 μs. From our measurements on electric field induced $P_{680}^+Q_A^-$ recombination (*38*) and arguments that will follow below, it appears that this charge pair is $P_{680}^+Q_A^-$. We will denote this EL by "EL(P)", as opposed to the "EL(Z)" generated by recombination of the radical pair $Y_Z^{ox}Q_A^-$ normally expected to be present in most PS II centers in this time range (*26*).

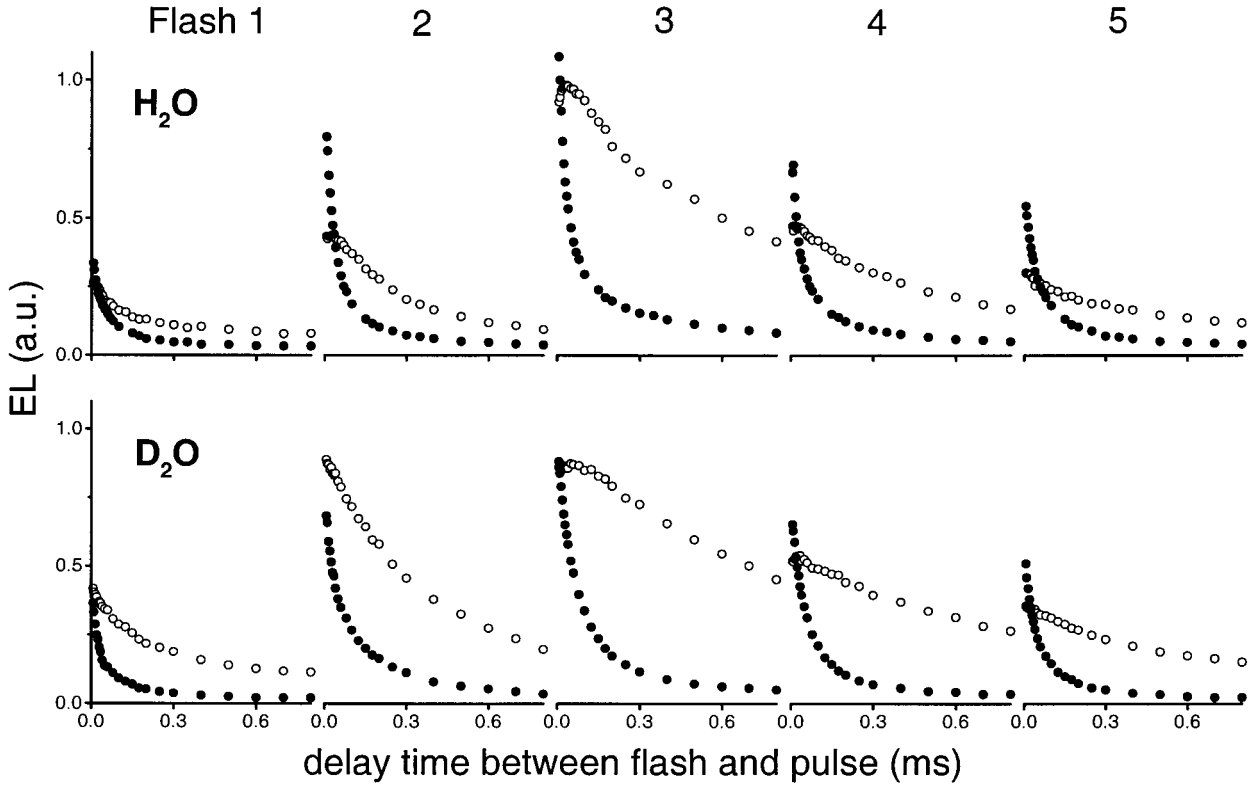

FIGURE 3: Early EL (solid circles) and late EL (open circles), measured as in Figure 2, as a function of the delay time (t_D) between flash and electric field pulse in H_2O (upper panels) and D_2O (lower panels). The early and late EL are plotted on the same scale, but note that the integration interval used for the late EL is 4 times longer (see text).

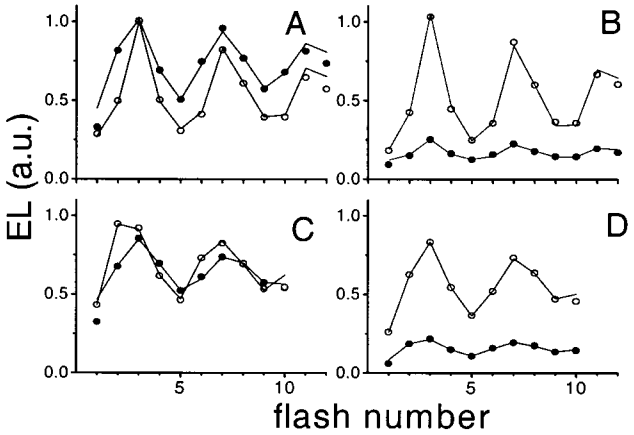

FIGURE 4: Early EL (solid circles) and late EL (open circles), measured as in Figure 2, as a function of flash number. (A) Blebs suspended in H_2O, $t_D = 10$ μs. (B) In H_2O, $t_D = 150$ μs. (C) In D_2O, $t_D = 10$ μs. (D) In D_2O, $t_D = 150$ μs. The lines represent fits as described in the text.

EL Oscillations with Flash Number. Figure 4 shows the flash number dependence of the early EL (solid symbols) and late EL (open symbols). The characteristic damped oscillations with a periodicity of 4 flashes show that both values are modulated by the S-state cycle of the oxygen-evolving complex. When the delay time between flash and pulse was short ($t_D = 10$ μs, Figure 4A), the S-state dependences of the early and late EL were clearly different. At a longer delay time ($t_D = 150$ μs, Figure 4B), the oscillation pattern of the early emission became more similar to that of the late emission, with a relatively lower amplitude on flash numbers 2, 6, and 10, but lower modulation depth. This is consistent with the interpretation that part of the early EL at this time after the flash is due to EL(Z), and indicates that the 100−200 μs decay of the early EL precursor shows little S-state dependence, as expected if it is due to charge recombination in inactive centers.

The lines in Figure 4A,B indicate the best simultaneous fit of the Kok model to all four oscillation patterns with a common, S-state-independent miss probability, which was found to be 8.6%. No double hits were allowed, in view of the short laser flashes used. All centers were assumed to start in state S_1 (*26*, *39*), and the S-state dependence of the EL emission was allowed to vary for each oscillation pattern. The data from flash numbers 11 and 12 were ignored in the fit: the deviation of these data results from Q_A^- accumulation when the plastoquinone pool is exhausted (*40*). The early EL after the first flash also had to be ignored. The deviation of this point may be explained by assuming that a small fraction of the centers lack a functional manganese cluster. In such centers, the first flash would produce a long-lived Y_Z^{ox}, and after subsequent flashes (at 10 Hz), a flash number independent $P_{680}^+Q_A^-$ recombination would be expected to contribute to the early EL, consistent with the observed 100−200 μs phase in the decay of the early EL precursor.

After replacement of H_2O by D_2O, the oscillations of both the early and the late EL with flash number were modified (Figure 4C,D). A good fit of the Kok model could be obtained in the same way (lines), if a slow conversion (1% per flash) of oscillating into nonoscillating centers was assumed. The best-fitting miss probability was 11.2%. The increase of the miss probability from 8.6 to 11.2% by H/D isotope exchange is in good agreement with results in ref (*23*). Earlier measurements by Arnason and Sinclair also

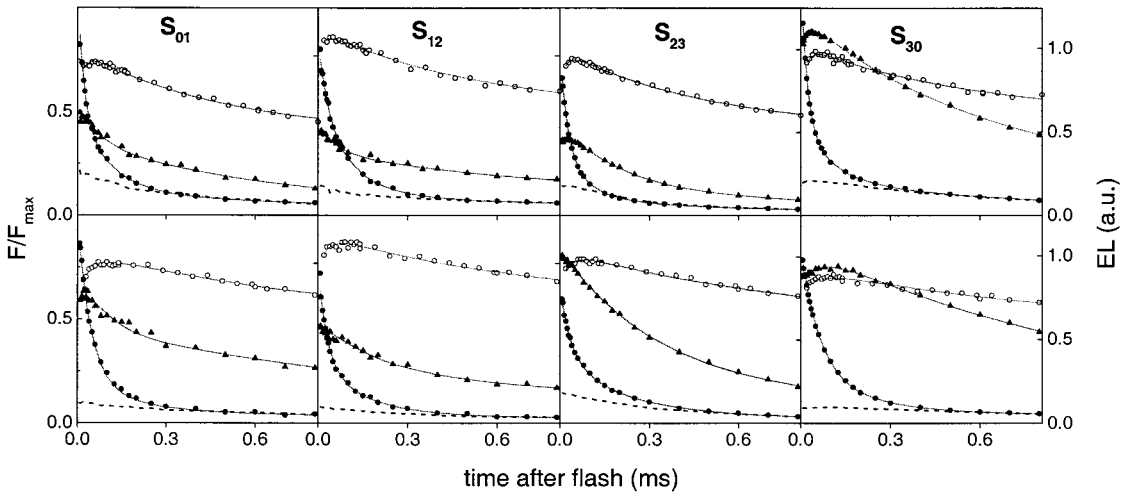

FIGURE 5: S-state decomposed data for the fluorescence (open circles, corresponding to the leftmost axis) and early EL (solid circles) and late EL (solid triangles) calculated from flashes 2−5 in Figures 1 and 3 and the S-state fit of Figure 4. The data for the S_{23} and S_{30} transitions correspond to the rightmost axis. For the S_{01} and S_{12} transitions, the data are shown on a 1.9 times expanded scale. Upper panels, blebs suspended in H_2O; lower panels, in D_2O. The dashed lines show late EL data normalized to the early EL data, indicating the upper limit for the contribution of EL(Z) to the early EL. The solid lines represent fits as described in the text.

indicated an increase in miss factor upon replacement of H_2O by D_2O (*41*).

If EL(P) originates largely from a different population of PS II centers than the bulk of EL(Z), the long-lived P_{680}^+ state in that population would be expected to cause an increased miss probability. For both the H_2O and the D_2O sample, a marginal improvement of the fit was obtained if the four patterns were fit separately. This resulted in a 1−1.5% *lower* miss probability for the early EL at $t_D = 10$ μs. Hence, the EL(P) dominating this emission does not come from a separate population of PS II centers with increased miss probability. Also, measurements at nonsaturating flash energy did not reveal a difference in antenna size for centers contributing to the early and late EL (not shown).

Kinetic Analysis. A detailed analysis of the early and late EL signals and fluorescence yield transients in both H_2O and D_2O was carried out to obtain a model for the underlying reaction kinetics and H/D exchange effects. Due to imperfect S-state turnover, the signals are a mix of contributions of the different S-states. Therefore, all measurements used were first decomposed using the relative S-state populations that were obtained by fitting the oscillation patterns as above. The result is shown in Figure 5; each decay curve now represents the kinetics that would be obtained when 100% of the PS II RC would be in the indicated S-state just before the flash. We will use the notation S_{01} etc. merely to indicate assignment of a kinetic phase to the $S_0 \rightarrow S_1$ transition by this decomposition, whatever the contribution to misses or S-state advancement of the reaction involved. In each frame, the lines represent the best simultaneous fit of EL data and fluorescence yield (fluorescence data with $t_D > 800$ μs are not shown in Figure 5). In the description of the fitting procedures and results below, we will deal with early EL, fluorescence yield, and late EL in that order, but it should be kept in mind that they were fit simultaneously and the resulting parameter values are somewhat interdependent.

(A) Fitting of the Early EL Data. To fit the decay of the early EL as a function of t_D, two exponentials and a small offset were necessary. In this case, amplitudes and time constants both depended significantly on S-state. For all four S-states, the time constants found were in the 20−60 and 100−200 μs range, respectively. However, the early EL must contain a contribution of EL(Z). An upper limit to this contribution can be found if it is assumed that the later stages of the early EL ($t_D > 600$ μs) consist entirely of EL(Z). The dashed lines in Figure 5 indicate this maximal contribution, calculated by normalizing the late EL to the early EL using the average of the last three points of the decay series.

It was found that the early EL data could not be fitted with a variable amount of EL(Z) contribution (using the shape of the late EL decay curve) and a single-exponential decay phase for EL(P). Still, two exponential decay components with time constants of 20−60 and 100−200 μs were necessary. In total, six parameters are available to describe the early EL decay: two amplitudes and two time constants for the EL(P) exponential decay functions, a contribution of EL(Z), and (possibly) an offset due to residual photosystem I EL. This set is overcomplete with respect to what is minimally required to describe the data, and this will result in cross-correlations between parameters. On the other hand, additional constraints are possible if we assume that the fast component in EL(P) decay and the initial rise component observed in the fluorescence and EL(Z) (for some S-states) all originate from the same process: stabilization of the charge separation by electron transfer from Y_Z to P_{680}^+. This allows us to simultaneously fit the early EL and the fluorescence yield. For the S_{23} and S_{30} transition in H_2O and the S_{30} transition in D_2O, resolved initial rise phases are observed in the EL(Z), and in these cases, the EL(Z) data were also included in the fit.

Amplitudes and time constants for both the fast (stab) and slow (rec) EL(P) components that were found in this way are listed in Table 1. In view of the expected cross-correlations, however, the best-fitting values may be quite unreliable. To deal with this problem, we used a Monte Carlo approach to obtain confidence distributions of the fit parameter as described under Materials and Methods. The result is shown in Figure 6 in the form of scatter diagrams illustrating, for each S-state transition, the confidence distribution of the amplitude and the time constant of the

Table 1: Amplitudes and Time Constants for the Two Decay Components of the EL(P) Precursor in H_2O and D_2O Found by Fitting the Early EL Data

	A_{stab} (a.u.)		τ_{stab} (ms)		A_{rec} (a.u.)		τ_{rec} (ms)	
	H_2O	D_2O	H_2O	D_2O	H_2O	D_2O	H_2O	D_2O
S_{01}	0.38	0.50	22	46	0.22	0.09	114	178
S_{12}	0.21	0.30	33	30	0.25	0.15	107	128
S_{23}	0.76	0.38	31	33	0.14	0.25	161	152
S_{30}	0.90	0.70	21	63	0.34	0.35	95	190

two EL(P) phases in H_2O (solid symbols) and D_2O (open symbols). We note again that the fits include fluorescence and EL(Z) data as in Table 1, with a shared time constant for the fast phase.

(B) P_{680}^+ Reduction Kinetics. In all cases, the confidence intervals of the time constants for stabilization and recombination are well separated. In H_2O, both time constants may be S-state-independent; their modulation by S-state is probably less than a factor of 2. Ambiguous results were obtained only for the S_{23} transition where the EL(Z) decay is not easily discriminated from the recombination component. The best fit was found in the tails of the distributions shown, with a 20 μs stabilization component, a 40−60 μs recombination component of similar magnitude, and a large (near-maximal) EL(Z) contribution. However, another fitting regime could be imposed by limiting the amount of EL(Z) contribution to about half the value obtained in the unconstrained fit, that still yielded satisfactory fits. In this case, the best fitting time constants for the stabilization and recombination components were 31 and 161 μs, respectively, with most of the amplitude in the stabilization component.

Suspending the blebs in D_2O instead of H_2O (Figure 6, open symbols) modified the S-state dependencies of both EL(P) components. For the S_{01} transition, the stabilization appears to be slower. S_{12} was not significantly changed. For the S_{23} transition, a large decrease of the amplitude of the stabilization and some increase in the amplitude of the recombination seem the most likely interpretation. If the recombination component in H_2O is really much faster, however, the main effect of D_2O is to slow that down. For the S_{30} transition, the D_2O effect appears to be different in nature: the stabilization component is slowed from 15 to 25 μs in H_2O to 50−75 μs in D_2O, and its amplitude is smaller. The recombination component is not significantly changed and remains distinct from the stabilization component.

(C) S_{12} Transition vs First Flash. Due to the presence of some inactive RCs, signals observed on the first flash in dark-adapted PS II differ from those calculated for the S_{12} transition by S-state decomposition of signals measured during subsequent cycles of the S-states. When acceptor-side electron transfer is blocked after Q_A^- (*42*), inactive centers are expected to contribute to the EL signal on the first flash but stay closed (high fluorescence) long enough to block a stable charge separation when subsequent flashes are fired at the 10 Hz flash frequency used. These RCs should not contribute to EL(P). On the PS II donor side, electron transfer from the manganese cluster may not occur. In this case, the RC should resemble RCs that were manganese-depleted by Tris-washing. Here, after the first flash, P_{680}^+ is reduced with a 15 μs time constant (pH 6.5) and produces a long-lived Y_Z^{ox}. If a second charge separation occurs while Y_Z is still oxidized, $P_{680}^+Q_A^-$ recombination is expected to occur with a 100−200 μs time constant. Hence, this component would contribute to the EL(P) after all flashes except the first, and appear as an S-state-independent 'contamination' in the S-state decomposed data.

To estimate the contribution of inactive RC to the recombination component in EL(P), the early EL on the first flash was compared to that found for the S_{12} transition (by decomposing the signals on flashnumbers 2−5). A good fit of the first flash was obtained with a smaller amplitude of the recombination component and a faster stabilization component than found for the S_{12} transition. When the time constant of the stabilization component was fixed at 33 μs (as found for the S_{12} transition), its amplitude was found to be the same as for the S_{12} transition, and an extra component was necessary to fit the early EL on the first flash. The time constant of this extra component was found to be 13 μs with an amplitude of 0.07 on the scale of Figure 6. The recombination component was found to be 0.15 unit lower than for S_{12}. The lower amplitude of the 13 μs component may indicate that the rate or EL yield of $P_{680}^+Q_A^-$ recombination is somewhat lower in the absence of Y_Z^{ox}. These findings are consistent with the presence of RCs with an inactive donor side. Presumably these RCs contribute about 0.15 unit to the recombination components in Figure 6. This estimate seems to be well in line with the deviation observed on the first flash in the oscillation patterns of Figure. 4. The recombination component cannot be due entirely to inactive centers. Indeed, Figure 6 shows that the amplitude of the recombination component in H_2O is significantly higher than 0.15 unit on the S_{30} transition. In D_2O, a higher amplitude of the recombination component is observed for the S_{23} and probably the S_{30} transition.

(D) Fitting of the Fluorescence Data. Fitting of the fluorescence was performed by relating *C*, the fraction of nonquenching RCs (with reduced Q_A^- and P_{680}), to fluorescence according to (*43*)

$$\frac{F}{F_M} = 1 - \frac{1 - C}{\frac{1}{\epsilon} - pC} \qquad (1)$$

where F = observed fluorescence, F_M = fluorescence corresponding to all RCs closed (3.7 times F_0, the fluorescence level in the dark-adapted sample, and assumed to be S-state-independent), $\epsilon = (F_M - F_0')/F_M$ (the trapping efficiency with open centers where F_0' corresponds to the fluorescence level with all Q_A oxidized *after* a particular flash), and p = probability of excitation transfer from a closed RC to another PS II (*44*) [corresponding to ω in (*43*)]. The value of p was set to 0.5, which is rather arbitrary. However, because fluorescence changes on all transitions were similar, changing p only shifted the absolute values of the parameters without affecting the relative relationships. The concentration of closed centers *C*, i.e., RCs with $P_{680}Q_A^-$, as a function of time after the flash was calculated assuming the following reaction scheme:

$$DP_{680}^+Q_A^- \xrightarrow{k_{stab}} D^+P_{680}Q_A^- \xrightarrow{k_Q} D^+P_{680}Q_A \qquad (2)$$

Here D denotes secondary donors to P_{680}^+, k_{stab} ($=1/\tau_{stab}$) is

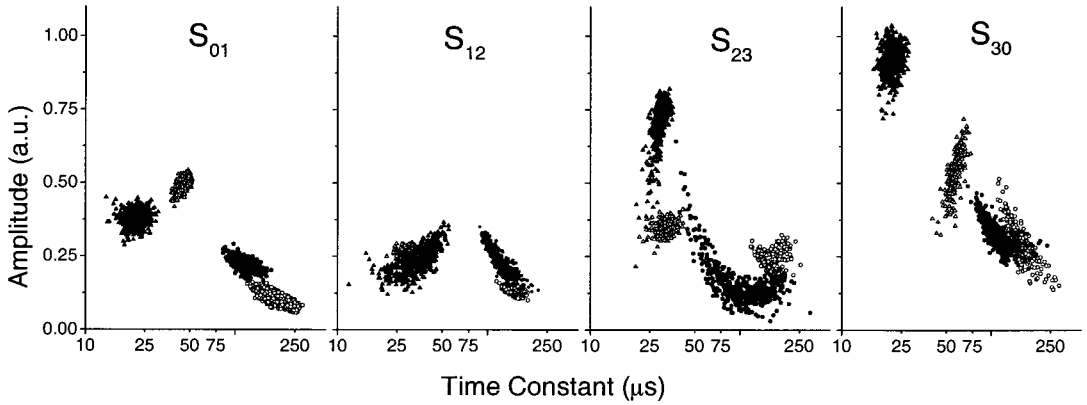

FIGURE 6: Confidence distributions/correlation diagrams for the parameters of the two EL(P) components. The distributions were obtained by a Monte Carlo fit simulation (see Materials and Methods). 500 synthetic datasets were generated based on the fit to the original data (Table 1). For each S-state transition, the amplitude/time-constant pairs are plotted for the fast (stabilization, triangles) and slow components (recombination, circles) for blebs suspended in H_2O (solid symbols) or D_2O (open symbols). Note the logarithmic scaling of the horizontal axis. Other fit parameters were an offset and EL(Z) contribution as described in the text.

the observed rate constant of P_{680}^+ reduction, and k_Q is the rate constant of Q_A^- oxidation by Q_B/Q_B^-.

The fluorescence kinetics are given by eq 1 with C the solution of the kinetics of the intermediate (high-fluorescent) state $D^+P_{680}Q_A^-$ (*45*):

$$C(t) = C(0)\cdot\exp(-k_Q t) + \frac{k_{stab}}{k_Q - k_{stab}}\cdot\{Q_0 - C(0)\} \{\exp(-k_{stab}t) - \exp(-k_Q t)\} \quad (3)$$

where $C(0)$ is the fraction of PS II initially in the state $D^+P_{680}Q_A^-$, assuming that all P_{680}^+ reduction faster than the 20−50 μs component is instantaneous. Q_0 = the total fraction of PS II that produces a stable charge separation ($D^+P_{680}Q_A^-$), either instantaneously or in 20−50 μs, and corresponds to the fluorescence yield obtained by extrapolating the fluorescence decay phases back to $t = 0$. The rate constant $k_{stab} = 1/\tau_{stab}$ of the 20−50 μs rise is shared with the fit to EL(P) data and to those EL(Z) data where the initial rise was resolved. Nevertheless, the amplitude of the rise $[Q_0 - C(0)]$ is very poorly defined at the time resolution of our fluorescence data: values of 10−50% of Q_0 were found.

The oxidation rate of Q_A^- by Q_B/Q_B^- is given by k_Q. To account for the biphasic decay of the fluorescence, a fraction with a fast Q_A^- decay (Q_B site occupied) and a fraction with a slow Q_A^- decay (Q_B site empty) were included in the fit. The P_{680}^+ reduction properties of both fractions were assumed to be equal. All fluorescence left after the slower phase is assumed to be due to open centers (F_0'). This assumption ignores the presence of a small amount of Q_A^- in equilibrium with Q_B^-. Consequently, in our fit the value of F_0' is overestimated. When an amount of 5% Q_A^- was added as an offset to eq 3, values of fit parameters shifted somewhat but not to the extent that our general conclusions were affected. The results of the Monte Carlo fit simulation are shown in Figure 7, retaining only the points for which the fraction of slow phase lies between 0 and 1.

(E) Q_A^- Oxidation Kinetics. In Table 2 the relative weight and time constants of the two phases of Q_A^- oxidation by Q_B/Q_B^- obtained by fitting the fluorescence yield decay are listed. The confidence intervals represented in Figure 7 show strong cross-correlations between parameters in both H_2O and D_2O, but some consistencies can be discerned. In H_2O, the time constants found for the fast component are in the 400−800 μs range and do not seem to depend much on whether mainly Q_B (S_{12}, S_{30}) or Q_B^- (S_{01}, S_{23}) is reduced by Q_A^-. The time constant of the slow component may be in the 2−5 ms range for all S-state transitions, but in the case of the S_{01} and S_{23} transitions, the possibility exists that it is significantly slower. The distributions indicate that the fraction of fast decaying Q_A^- is smaller for Q_B than for Q_B^- reduction.

In D_2O, the decay of Q_A^- is significantly slower than in H_2O. This retardation appears to be larger for the S-state transitions associated with Q_B^- reduction. Here the data could be fitted using the assumption either that the time constant of the slow component or that the value of F_0' remained unchanged by H_2O/D_2O exchange. A larger value of F_0' in D_2O would indicate a temporary (no longer seen at 100 ms) decrease of trapping efficiency by plastoquinol formation in D_2O but not in H_2O. This seems rather unlikely. Therefore, we used the alternative assumption for fitting the D_2O data and fixed the value for F_0' to the value found in H_2O (Table 3) for all S-states. The results of fitting the data using this assumption can be seen in Table 2 and Figure 7. For the S_{12} and S_{30} transitions, the retardation is due to a slight decrease in the rate of the fast component and/or an increase of the fraction of RC decaying by the slow component. For the S_{01} and S_{23} transitions, the retardation results from a significantly slower rate of Q_A^- oxidation in the fast phase and time constants for the slow component that were much larger than the 2−5 ms possible in H_2O. For the S_{01} transition, a good determination of this time constant is not possible from the data because the fitted value tends to become very large; part of the distribution is off-scale in Figure 7.

Table 3 presents best-fit values and confidence intervals for $1 - Q_0$ as a function of S-state. This value corresponds to the fraction of RCs where $P_{680}^+Q_A^-$ recombination occurred, about 12% on the S_{12} transition and about 22% on the other S-state transitions. The main effect of H_2O/D_2O exchange is on the S_{30} transition, where a value of approximately 30% is found. The 8% extra misses on S_{30} account for most of the 2.6% higher miss probability in D_2O found from the oscillation patterns in Figure 4. The average amount of recombination is higher than the average miss

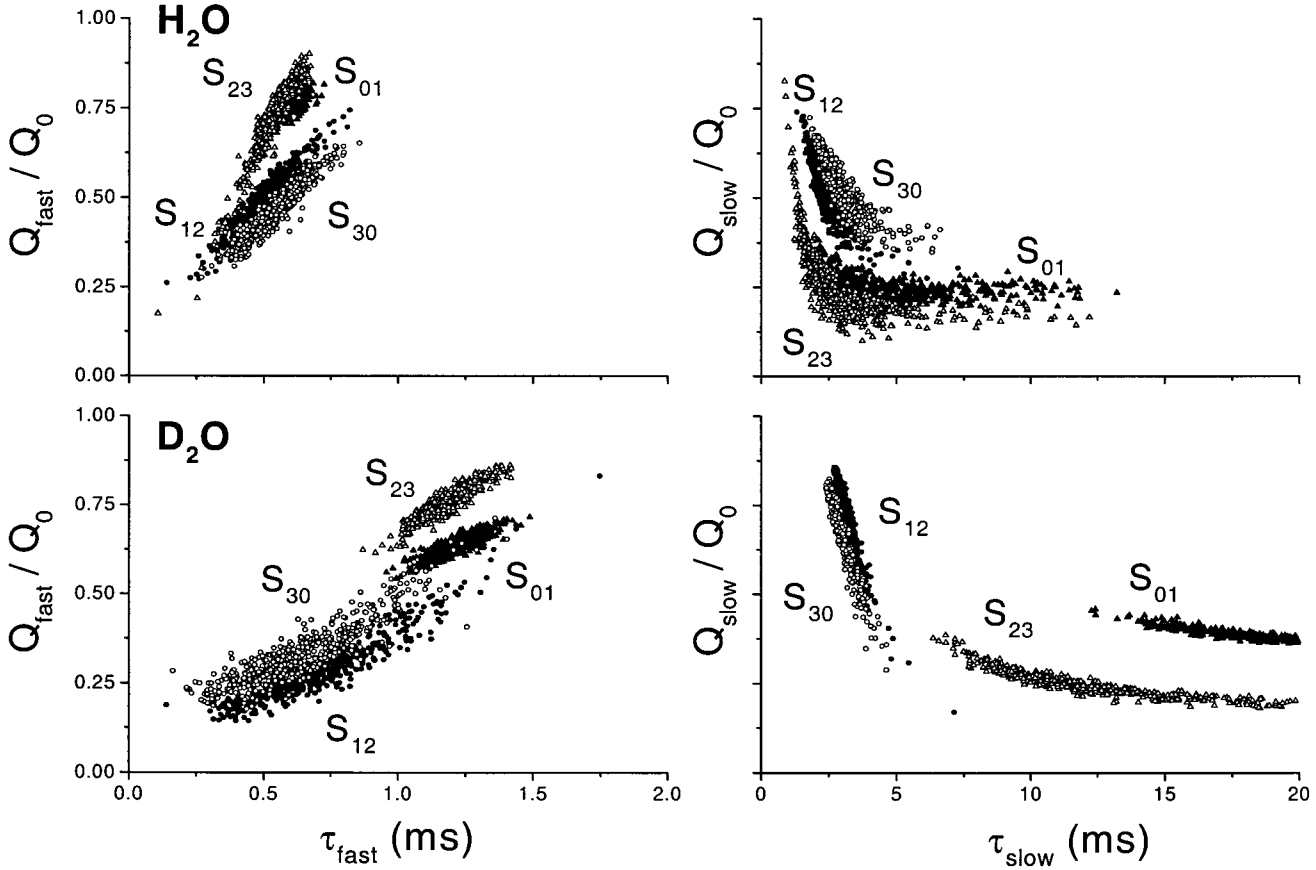

FIGURE 7: Confidence distributions/correlation diagrams as in Figure 6 for parameters fitted to the fluorescence data as described in the text. Plotted are the distributions obtained for the amplitude and time constants of the fast (τ_{fast}, left panels) and the slow component (τ_{slow}, right panels) of Q_A^- oxidation in H_2O (upper panels) and D_2O (lower panels). Data belonging to the S-state transitions as indicated: S_{01}, solid triangles; S_{12}, solid circles; S_{23}, open triangles; S_{30}, open circles.

Table 2: Relative Amplitudes and Time Constants for Q_A^- Oxidation Found from the Flash-Induced Fluorescence Yield Changes in H_2O and D_2O

	$Q_{fast}/(Q_{fast}+Q_{slow})$		τ_{fast} (ms)		τ_{slow} (ms)	
	H_2O	D_2O	H_2O	D_2O	H_2O	D_2O
S_{01}	0.78	0.72	0.63	1.4	5.6	∞
S_{12}	0.48	0.26	0.48	0.68	2.3	3.1
S_{23}	0.78	0.76	0.56	1.2	2.6	12.1
S_{30}	0.46	0.30	0.46	0.60	2.8	2.9

Table 3: Values of Fit Parameters Found by Fitting the Fluorescence As Described in the Text for the Four S-State Transitions in Blebs Suspended in H_2O and D_2O[a]

	$1-Q_0$		F_0'	
	H_2O	D_2O	H_2O	D_2O
S_{01}	0.22 (0.20−0.23)	0.18 (0.16−0.19)	1.12 (1.02−1.19)	1.12 fixed
S_{12}	0.12 (0.08−0.14)	0.12 (0.10−0.14)	1.46 (1.41−1.50)	1.46 fixed
S_{23}	0.23 (0.22−0.25)	0.20 (0.18−0.21)	1.31 (1.24−1.36)	1.31 fixed
S_{30}	0.21 (0.19−0.23)	0.29 (0.25−0.32)	1.33 (1.25−1.38)	1.33 fixed

[a] $1-Q_0$ is the fraction of RC's that undergo $P^+_{680}Q_A^-$ recombination. F_0' is the fluorescence yield of an open RC some milliseconds after a flash normalized to the fluorescence yield of a dark-adapted preparation; for the D_2O data, it was fixed to the value found in H_2O (see text). The 95% confidence intervals of the parameter values are shown in parentheses.

probability by 9−11% in H_2O as well as D_2O, which must be attributed to nonoscillating (inactive) RCs that undergo $P_{680}^+Q_A^-$ recombination on each flash. These numbers would imply that the miss probability on the S_{12} transition is small and charge recombination in the microsecond time domain accounts for most of the misses on the other S-state transitions.

(F) EL(Z) Decay. In H_2O, the EL(Z) decay for the lower two S-states is biphasic. The fast rate is found to be 20−120 μs for both S-states, and most likely corresponds to the S-state transition. In D_2O, the rate is found to be much slower (300−400 μs), but the slower phase is no longer resolved separately so that comparison becomes difficult. Furthermore, for the S_{01} transition, a low weight initial rise phase may be included in the fit, resulting in faster decay rate. For the S_{23} transition, the EL(Z) decay rate is 200−300 μs in H_2O and 300−400 μs in D_2O. The S_{30} transition shows an EL(Z) decay of 600−800 μs in H_2O. In these cases, unresolved slower phases are treated as an offset. In D_2O, the EL(Z) decay on S_{30} is retarded such that a reasonable estimate of its decay rate becomes impossible. The extraction of Y_Z^{ox} reduction times from these data will be treated under Discussion.

DISCUSSION

The results presented here confirm the suggestion by Vos et al. (*26*) that EL induced in PS II within a few tens of microseconds after a flash contains a large contribution from a charge pair that is less stable than $Y_Z^{ox}Q_A^-$ and that is

more rapidly exhausted during the electric field pulse. The most likely candidate for such a charge pair would be $P_{680}^{+}Q_A^{-}$. Our EL measurements on Tris-treated PS II (*38*) demonstrated the feasibility of studying the kinetics of $P_{680}^{+}Q_A^{-}$ recombination, which showed similarly rapid kinetics during the pulse. Making use of the distinction between "EL(P)" from $P_{680}^{+}Q_A^{-}$ and "EL(Z)" from $Y_Z^{ox}Q_A^{-}$, EL(P) was studied in oxygen-evolving samples. Detailed information was obtained on the S-state dependence and susceptibility to H_2O/D_2O exchange of the well-known but poorly understood 20−30 and 100−200 μs components in the reduction of P_{680}^{+}.

Kinetics of EL Emission during the Pulse. Although EL was used only as a probe to measure the amount of a particular state at a certain time after the flash, some remarks on the kinetics of EL emission during the pulse (Figure 2) are in order because they were used to distinguish $P_{680}^{+}Q_A^{-}$ from $Y_Z^{ox}Q_A^{-}$. For optimum selectivity, "early EL" was taken as early as possible during the pulse, at the initial rise of the signal (due to the sigmoid rise of the signal, inclusion of the first 5 μs would add mainly noise). The rise kinetics reflect the build-up of the membrane potential and depend on the specific resistance of the medium and the size of the blebs, both of which might be changed by making blebs in D_2O rather than H_2O. Significant differences in the initial rise kinetics of the signal were not detected, however, so the observed effects of H_2O/D_2O exchange cannot be attributed to modified characteristics of the membrane potential.

"Late EL" was taken as the signal integrated during the last 20 μs of the 180 μs pulse. The relative amplitudes of early and late EL as defined in this study cannot be used to estimate the relative amounts of $P_{680}^{+}Q_A^{-}$ and $Y_Z^{ox}Q_A^{-}$ present at the onset of the pulse. This is because they depend not only on the integration interval and time course of the EL emission but also on the different activation energies and field strength dependencies of charge recombination from these two states. Moreover, the late EL amplitude also depends on changes in the precursor concentration caused by the electric field during the first 160 μs of the pulse. Such an effect on the late EL amplitude is observed at very short t_D, when the slow phase of P_{680}^{+} reduction by Y_Z is not finished yet. The electric field increases the probability that this fraction of P_{680}^{+} is lost by recombination before it oxidizes Y_Z, resulting in a decrease of the late EL emission measured 160 μs later. As a result, the slow stabilization phase was reflected in an initial rise of late EL as a function of t_D on the S_{30} transition and, in H_2O, on the S_{23} transition as well, but not well resolved in the other cases. Reaction dynamics during the electric field will determine how much of the slow Y_Z oxidation is prevented, so the relative extent of the initial rise in the late EL gives only a minimum estimate of the fraction of PS II involved in the slow stabilization process.

On the S_{23} transition in D_2O, the EL(Z) emission is doubled with respect to that in H_2O, apparently at the expense of EL(P). This suggests that D_2O shifts the quasi-equilibrium between $P_{680}Y_Z^{ox}$ and $P_{680}^{+}Y_Z$ during the pulse toward oxidized P_{680}. Such a shift would also double the rate of charge recombination. No net acceleration is observed when the EL(Z) kinetics during the pulse for the S_{23} transition are compared for H_2O and D_2O, but there is also no retardation of the decay similar to that observed on the other flashes in Figure 2 and expected because of the retardation of electron transfer beyond Y_Z^{ox} and Q_A^{-} (Figure 7 and Table 4). The EL(Z) decay on the other flashes is approximately 1.5 times slower in D_2O than in H_2O. A 2-fold faster recombination would just compensate that on the second flash if the recombination reaction accounts for approximately one-third of the total EL decay rate during the pulse (in H_2O on the second flash), which seems reasonable. The observation of a concomitant decrease of EL(P) by D_2O suggests that the apparent equilibrium constant $[P_{680}Y_Z^{ox}]:[P_{680}^{+}Y_Z]$ is quite small during the pulse [electron transfer between P_{680} and Y_Z is known to be electrogenic (*46*)]. The fraction of early EL attributed to the slow stabilization component of EL(P) depends on how much P_{680}^{+} remains pulse-inducible at later t_D, in quasi-equilibrium with Y_Z^{ox}. For instance, if the slow stabilization involves 30% P_{680}^{+}, 10% P_{680}^{+} should be pulse-inducible in equilibrium with Y_Z^{ox} in H_2O, and 20% in D_2O, to explain that the amplitude of the stabilization component of EL(P) is halved while EL(Z) is doubled by D_2O on the S_{23} transition. It is not clear why D_2O specifically destabilizes $Y_Z^{ox}S_2$, but a factor of 2 corresponds to a potential shift of only 20 mV. It is perhaps more surprising that D_2O has even less influence on the potential of Y_Z in the other S-states.

Table 4: Time Constants (μs) for Y_Z^{ox} in Reduction by the Manganese Cluster As Determined from a Fit as Described in the Text[a]

	H_2O	D_2O	ref (*57*)	ref (*58*)
S_{01}	61 (55−75)	61 (50−90)	43	360
S_{12}	53 (35−75)	179 (150−200)	160	55
S_{23}	261 (200−370)	379 (360−400)	500	420

[a] The model used for fitting the EL(Z) included the kinetics of Q_A^{-} oxidation taken from Table 2 and the rate of the stabilization phase of P_{680}^{+} taken from Table 1. For the S_{01} and S_{12} transitions, Q_A^{-} oxidation accounted for the second decay phase observed on our time scale (see text). Error margins were estimated by varying the fixed parameters over their confidence intervals. The listed literature values for the time constants are calculated from the half-times (in H_2O) reported by the authors.

Heterogeneity. In most PS II centers, the state $Y_Z^{ox}Q_A^{-}$ is formed in less than the 15 μs delay between the flash and the 'early EL' measurement. $P_{680}^{+}Q_A^{-}$ is detected only to the extent that it persists in quasi-equilibrium with $Y_Z^{ox}Q_A^{-}$, and in centers that fail to oxidize Y_Z in that time. In all cases, two clearly distinct components of 20−50 and 100−200 μs were found in the decrease of EL(P) as a function of the delay time between the flash and the electric field pulse. They correspond to slow phases in the reduction of P_{680}^{+} that are attributed to a slow reduction by Y_Z and recombination with Q_A^{-}, respectively. To which extent the heterogeneous P_{680}^{+} reduction kinetics reflect a 'static' or 'dynamic' heterogeneity of PS II is not clear from the literature, and the answer may well depend on the material and experimental conditions used. Some PS II centers that lack a functional Mn cluster and remain inactive on a time scale of seconds represent the only static heterogeneity seen under our experimental conditions [inactive centers blocked at the acceptor side would not show up in EL(P) or EL(Z)]. We found that the miss probability in the period 4 oscillation with flash number is

not higher for EL(P) than for EL(Z), whereas most misses appeared to be due to charge recombination during the slow P_{680}^+ reduction phases. This implies that the population of active PS II RCs involved in EL(P) or EL(Z) is randomly redistributed between flashes, placing an upper limit of tens of milliseconds on the redistribution time. However, this result does not distinguish a dynamic heterogeneity due to 'effective and ineffective stabilizers' that redistribute in 10 ms, as reported by Lavergne and Rappaport (*47*), from an essentially homogeneous submicrosecond equilibration between $P_{680}^+Y_Z$ and $P_{680}^+Y_Z^{ox}$ followed by a 30 μs relaxation, as proposed by Rappaport et al. (*48*).

The Recombination Component. The presence of some 'inactive' PS II centers that lack a functional oxygen-evolving complex is probably inevitable in all preparations, and introduces a static heterogeneity. The kinetic properties of such centers are well-known, however, and if their contribution is the same on all flashes in a series except the first, the only problem is to determine the amplitude of that contribution. The presence of these centers under the conditions used here was demonstrated by the difference in EL(P) kinetics after the first flash and that obtained for the S_{12} transition in active centers. Approximately 11−12% inactive centers had to be assumed to explain the fluorescence data. The main uncertainty in this number is the estimated degree of nonlinearity between fluorescence yield and Q_A concentration. A reasonable error of 0.2 in the connectivity parameter of 0.5 would not increase the possible range for the amount of inactive PS II beyond 9−15%.

Although charge recombination in inactive centers accounts for most of the amplitude of the 100−200 μs decay of EL(P) in lower S-states, no acceptable fit could be obtained if this component was assumed to be S-state-independent. The confidence distributions in Figure 6 show that it was significantly larger than the estimated contribution of inactive centers on S_{30} and in D_2O also on S_{23}. This cannot be attributed to a gradual inactivation during the flash series, because the information on S_{01} and S_{12} was obtained from flash numbers 4 and 5, after the higher S-state transitions. A 100−200 μs component was also resolved in refs (*13*, *22*) by absorbance difference measurements, but there it could be treated as S-state-independent. This difference is most likely due to the lower signal-to-noise ratio of those measurements. Our data show that active, oxygen-evolving centers contribute to the 100−200 μs phase in P_{680}^+ reduction on the S_{30} transition. We found no indication for a concomitant increase in fluorescence yield or EL(Z), so this contribution to the 100−200 μs EL(P) decay is also most likely due to charge recombination of $P_{680}^+Q_A^-$. Since the recombination time was not distinguishable from that in inactive centers, it may be justified to conclude from the approximately 2-fold larger total amplitude of the slow component on the S_{30} transition that the number of active centers involved is comparable to the number of inactive centers. We conclude that, at least in the conditions used here, a substantial part of the miss probability on the S_{30} transition in H_2O may be due to a 100−200 μs charge recombination taking place in a statistical fraction of the active reaction centers.

Y_Z must be temporarily unavailable for oxidation in these centers, and the simplest explanation would be the presence of some $Y_Z^{ox}S_2$ in equilibrium with Y_ZS_3. A charge separation in this case would recombine faster than it can be stabilized, if the presence of P_{680}^+ does not accelerate the reduction of Y_Z^{ox} by S_2. The same may apply to the $Y_Z^{ox}S_1/Y_ZS_2$ transition in D_2O but not in H_2O (Table 4). The reduction of Y_Z^{ox}, if unmodified, should still be fast enough to allow stabilization of a significant fraction of centers, and cause some fluorescence rise and a faster P_{680}^+ decay than in inactive centers. These effects, if present, were too small to detect. Other mechanisms that might cause a temporary inactivation of PS II and could explain the 100−200 μs charge recombination in oxygen-evolving centers cannot be ruled out. The 10 ms equilibration between 'effective and ineffective stabilizers' described by Lavergne and Rappaport (*47*) may reflect such a process. However, the S-state dependence constitutes an important restriction on possible mechanisms. For instance, dissociation of the essential chloride ion might specifically inactivate the S_3 state (*49*), but it would still allow Y_Z oxidation and cannot explain the recombination on the S_{30} transition.

The Slow Stabilization Process. Most of the slow P_{680}^+ reduction took place in the '35 μs' phase. The time constant was more likely 20−30 μs in our measurements, although it could be larger on S_{12} (Figure 6). The strong S-state dependence of the amplitude is similar to that observed in transient absorption spectroscopy (*22*), so it reflects mainly differences in the amount of P_{680}^+ involved. The effects of D_2O were also strongly S-state-dependent. The D_2O-induced decrease of the EL(P) amplitude on the S_{23} transition may be a consequence of the 2-fold increase of the EL(Z) on this transition, if the equilibrium constant $[P_{680}Y_Z^{ox}]:[P_{680}^+Y_Z]$ is small during the pulse. Note that this could apply both in the relaxing equilibrium model and in the case of a temporary heterogeneity. The slow stabilization is clearly slowed by D_2O on the S_{30} transition and apparently also on the S_{01} transition. The latter case is not very convincing, because the amplitude of the recombination component obtained for S_{01} in D_2O seems too small to accommodate the inactive centers, and a larger amplitude of the recombination component correlates with a smaller time constant of the stabilization component in the confidence distributions. However, it appears that the rate here is significantly slower in D_2O. On the S_{30} transition, retardation of stabilization is obvious and can also be seen in the shape of the EL signals measured 10 μs after the third flash (Figure 2).

D_2O also caused a ~10% lower overall yield of stable charge separation on the S_{30} transition (Table 3). The recombination component seems unaffected (Figure 6), so the lower yield in D_2O would have to be due to losses by recombination of $Y_ZP_{680}^+Q_A^-$ during the slow stabilization process. The loss probability is equal to the fraction of active PS II centers involved times the net observed τ_{stab} divided by the unknown time constant for the competing recombination of $Y_ZP_{680}^+Q_A^-$. The confidence distributions in Figure 6 show that τ_{stab} must be close to its best-fitting value of 20 μs in H_2O and 60 μs in D_2O. If $Y_ZP_{680}^+Q_A^-$ is assumed to recombine with a 150 μs time constant, like $Y_Z^{ox}P_{680}^+Q_A^-$, involvement of 37% of PS II in slow P_{680}^+ reduction would be needed to explain the 10% more losses in D_2O than in H_2O, which would then amount to 15% and 5%, respectively. The fraction of PS II involved in the slow fluorescence rise and maximally in the EL(Z) rise would be the remaining 22% (D_2O) or 32% (H_2O), consistent with the data. In this

example, the time constant calculated for the stabilization process itself is 100 μs in D_2O and 23 μs in H_2O, so the H/D effect is 4.3. Different $Y_Z P_{680}^+ Q_A^-$ recombination times may be assumed, but values larger than 300 μs [see, for instance, ref (*5*)] cannot explain the 10% losses in D_2O on the S_{30} transition, even if half of the centers show slow P_{680}^+ reduction.

We conclude that the competition between back-reaction and slow stabilization explains the increased miss probability in D_2O. The same conclusion was proposed by Christen et al. (*22*), but they could not rule out the alternative that the recombination component was increased at the expense of the stabilization component, because in D_2O the two components could not be resolved. The confidence distributions in Figure 6 show that in our analysis the two components could be resolved and that the stabilization is slowed. In addition, the amplitude of the stabilization component is decreased by D_2O, but no corresponding increase of the recombination component is observed.

The calculation of losses by recombination during the slow stabilization process remains the same if heterogeneity is involved or not. When the slow stabilization process involves the relaxation of an initial equilibrium between $P_{680}^+ Y_Z$ and $P_{680} Y_Z^{ox}$, as proposed in (*48*), the associated equilibrium constant K should be S-state-dependent and amount to 1.7 in the S_3 state to retain a fraction of $1/(K + 1) = 0.37 P_{680}^+$ before the stabilization process begins. The S-state dependence of K might be expected to influence the observed stabilization rate, but the differences would not exceed the confidence intervals obtained for this parameter. In case of a dynamic heterogeneity, an S-state-dependent fraction of up to 37% of PS II in S_3 must be unable to oxidize Y_Z in submicrosecond times, but does so in 20−30 μs with an efficiency of at least 80% (observed τ_{stab} 30 μs, τ_{rec} 150 μs). This is very different from the 10−20% efficiency of the 'bad stabilizers' of Lavergne and Rappaport (*47*). In view of the reported pH dependence of the amount of P_{680}^+ involved in the '35 μs phase' (*12*) and the evidence that Y_Z oxidation depends on the availability of the D1-His190 residue as a proton acceptor (*20*), it seems possible that protonation of this residue blocks the nanosecond reduction of P_{680}^+ and that its deprotonation is the rate-limiting step in the 20−30 μs reduction of P_{680}^+. However, any mechanism postulated to explain the 20−30 μs component must account for the fact that the rate is substantially decreased by D_2O in the S_3 state, perhaps to a lesser extent in the S_0 state, but probably not at all or much less in S_1 or S_2.

Q_B/Q_B^- Dependence of Q_A^- Oxidation Kinetics. The results of our analysis suggest that the redox state of Q_B in H_2O does not affect the rate constant of Q_A^- oxidation, as originally proposed by Bowes and Crofts (*34*), but instead affects the extent to which Q_A^- is oxidized during the fast phase. It is generally assumed that the slow phase reflects the oxidation of Q_A^- that is rate-limited by the diffusion of plastoquinone into the Q_B binding pocket. Conclusive evidence for this interpretation is not availabe, but it is supported by the fact that the slow component has its largest amplitude on the S_{12} and S_{23} transition where mainly Q_B reduction (and not Q_B^- reduction) is expected to occur. Q_B^- is supposed to be tightly bound to the PS II RC whereas Q_B is not (*50*, *51*), so the fraction of centers with an empty Q_B binding site should be largest on these transitions.

Replacement of H_2O with D_2O significantly retards oxidation of Q_A^-. To our knowledge, there is only one previous report on an H/D exchange effect on Q_A to Q_B electron transfer in PS II, and flash number dependence was not considered (*37*). We find that that the largest retardation of the fast phase of Q_A^- decay takes place on the S-state transitions where Q_B^- reduction is expected to dominate (S_{01}, S_{23}). This seems in line with the notion that this reaction requires prior protonation of the semiquinone (*52*), but on the other hand, that was found to be not rate limiting in the bacterial RC (*53*). The slow phase appears to respond to D_2O in a different way on the S_{01} and S_{23} transitions than on S_{12} and S_{30}. The strong retardation might indicate a decreased relaxation of the equilibrium between $Q_A^- Q_B^-$ and $Q_A Q_B H_2$, for instance due to a retarded release of plastoquinol from the Q_B pocket. However, this process is largely beyond the time scale of our data, and we cannot rule out a possible decomposition artifact. The amount of slow phase assigned to the S_{01} and S_{23} transitions depends on the presence of S_0 in the dark. This is negligible in the bleb wall (*26*, *39*) but unknown in the dense patches of thylakoid material seen on the bleb surface which contribute to the fluorescence but not to the EL (*26*, *39*, *54*, *55*).

Y_Z^{ox} Reduction Kinetics. As pointed out by Vos et al. (*26*), EL from the state $Y_Z^{ox} Q_A^-$ is expected to decrease as a function of t_D with the sum of the rate constants of Q_A^- oxidation and Y_Z^{ox} reduction. Compared to that study, the distinction between EL(P) and EL(Z) and the independent information on the oxidation kinetics of Q_A^- discussed above should allow a more reliable estimate of the S-state transition times from the EL(Z) data, at least to the extent that they take place in the 800 μs time range studied. The biphasic decay kinetics of EL(Z) on the S_{01} and S_{12} transitions indicate that the late EL in this time range actually does not disappear with Y_Z^{ox} and a substantial amount EL emission can still be induced in the state $S_{i+1} Y_Z$ initially formed, also on the S_{01} transition. Its decrease in the first millisecond is fully accounted for by Q_A^- oxidation (see below), but on a time scale of seconds, EL from S_0 and S_1 is negligible compared to that from the higher S-states (*26*). Apparently the S_0 and S_1 states are stabilized by a process that takes many milliseconds, and the electric field can efficiently regenerate Y_Z^{ox} until that has happened. Electrogenicity of electron transfer between Y_Z and the manganese cluster was previously reported in refs (*26*, *56*).

A kinetic model was set up to extract the rate of Y_Z^{ox} reduction from the EL(Z) data that took into account the kinetics of Q_A^- oxidation and possible contributions to the EL(Z) from $S_{i+1} Y_Z$; i.e., the slow phase observed in the EL(Z) decay for the S_{01} and S_{12} transitions was included as resulting from $S_{i+1} Q_A^- \rightarrow S_{i+1} Q_A$. An initial rise phase due to the reduction of P_{680}^+ was also included. Fit parameters were the rate of Y_Z^{ox} reduction and amplitudes for EL from the states $Y_Z^{ox} Q_A^-$, $S_{i+1} Q_A^-$, and an offset.

It was found that this model was able to describe the late EL data for the S_{01}, S_{12}, and S_{23} transitions; S_{30} was too slow to resolve. Results for the rates of Y_Z^{ox} reduction are listed in Table 4. Although the modeling is somewhat involved, the results for H_2O are in reasonable agreement with previous reports. Y_Z^{ox} reduction rates previously reported by Dekker et al. (*57*) and Rappaport et al. (*58*) are listed in Table 4 for reference. Between the two reports major discrepancies exist

concerning the rates of the S_{01} and S_{12} transitions. Our result is in accord with (*57*) for S_{01} and with (*58*) for the S_{12} transition. If we ignore the biphasicity of EL(Z) decay, as in Vos et al. (*26*), larger time constants for Y_Z^{ox} reduction are obtained, but the fits are poorer.

H/D exchange effects on the rate of Y_Z reduction by the manganese cluster have attracted some attention in view of the proposed hydrogen atom abstractor model. From EPR (*59*), optical measurements (*60*, *61*), and oxygen yield measurements (*41*, *62*), H/D isotope exchange effects are modest. There is some conflict in the literature concerning the magnitude of the isotope effect of the S_{12} transition and S_{23} transition. In the EPR experiments, a substantial kinetic isotope effect is observed for the S_{12} transition that is not apparent from the optical measurements. In the optical experiments, a kinetic isotope effect is observed for the S_{23} transition in isolated PS II core complexes but not in membrane fragments. Our result is in accord with the EPR measurements of Lydakis-Simantiris et al. (*59*): $k_H/k_D = 3-5$ for the S_{12} transition; $k_H/k_D = 1-2$ for the S_{23} transition. For the S_{01} transition, we find no isotope effect. Isotope effects on the S_{30} transition cannot be determined on the time scale of our measurements.

Concluding Remarks. The kinetics of secondary reactions in the microsecond time domain in active, oxygen-evolving PS II reflect the oxidation of Q_A^- by Q_B/Q_B^- and the reduction of Y_Z^{ox} by the oxygen-evolving complex, but also a 20−30 μs component of P_{680}^+ reduction by Y_Z and a 100−200 μs recombination of $P_{680}^+Q_A^-$ can be detected in a significant fraction of reaction centers.

On the PS II acceptor side, H_2O/D_2O exchange caused a 2-fold slower oxidation of Q_A^- by Q_B^- and appeared to influence the affinity of the Q_B binding pocket for plastoquinone and plastoquinol. On the donor side, all effects of D_2O were highly S-state-specific. The reduction of Y_Z^{ox} was unchanged on the S_{01} transition, 3−5-fold retarded on the S_{12} transition, and 1−2-fold retarded on the S_{23} transition. D_2O decreased the equilibrium constant between $P_{680}^+Y_ZS_2$ and $P_{680}Y_Z^{ox}S_2$ by a factor of about 2, whereas no such effect was seen on the other S-states.

The 100−200 μs $P_{680}^+Q_A^-$ recombination is tentatively attributed to the presence of some Y_Z^{ox} present in equilibrium with the S_i state, because it was significant when the reduction time of Y_Z^{ox} by S_{i-1} exceeded that of $P_{680}^+Q_A^-$ recombination: in the S_3 state and in D_2O also in the S_2 state. The 20−30 μs phase in the reduction of P_{680}^+ by Y_Z occurs in all S-states to different extents, and causes some misses due to the competing $Y_ZP680^+Q_A^-$ recombination, which must have a time constant lower than 300 μs. However, even when most RCs are involved, as may be the case when a large pH gradient is built up during steady-state photosynthesis, it will not cause more than 20% misses. The origin of this component remains unclear. As a possible alternative to the proposed relaxation after nanosecond equilibration of $P_{680}^+Y_Z$ and $P_{680}Y_Z^{ox}$, we suggest that the proton acceptor for Y_Z oxidation, presumably D1-His190, may already be in the protonated state in a fraction of the centers at the moment of charge separation and the 20−30 μs process may be its deprotonation. A coupling to proton transfer is suggested by the reported pH dependence of its amplitude and the 4-fold retardation of the process by D_2O on the S_{30} transition, causing 10% extra misses. However, the absence of an D_2O effect in S_1 and S_2 does not support the idea of a rate limitation by proton or hydrogen atom transfer on all S-state transitions.

ACKNOWLEDGMENT

We thank C. F. Yocum for valuable advice. We dedicate this paper to the memory of three admired scientists and dear friends who died after its submission: Prof. Gerald T. Babcock, whose insistence on the hydrogen atom abstraction model for water oxidation inspired this study; Prof. Bart G. de Grooth, who pioneered electroluminescence research in our laboratory; and Prof. Jan Amesz, who would have been promotor, for the last time, for the doctoral thesis of R.d.W. of which this work is part.

REFERENCES

1. Diner, B. A., and Babcock, G. T. (1996) in *Oxygenic Photosynthesis: The Light Reactions* (Ort, D. R., and Yocum, C. F., Eds.) pp 213−247, Kluwer Academic Publishers, Dordrecht.
2. Brettel, K., Schlodder, E., and Witt, H. T. (1984) *Biochim. Biophys. Acta 766*, 403−415.
3. Conjeaud, H., and Mathis, P. (1980) *Biochim. Biophys. Acta 590*, 353−359.
4. Conjeaud, H., Mathis, P., and Paillotin, G. (1979) *Biochim. Biophys. Acta 546*, 280−291.
5. Diner, B. A., Force, D. A., Randall, D. W., and Britt, R. D. (1998) *Biochemistry 37*, 17931−17943.
6. Reifarth, F., Renger, G., and Christen, G. (1997) *Photosynth. Res. 51*, 231−242.
7. Gerken, S., Dekker, J. P., Schlodder, E., and Witt, H. T. (1989) *Biochim. Biophys. Acta 977*, 52−61.
8. Zankel, K. L. (1971) *Biochim. Biophys. Acta 245*, 373−385.
9. Zankel, K. L. (1973) *Biochim. Biophys. Acta 325*, 138−148.
10. Eckert, H. J., and Renger, G. (1980) *Photochem. Photobiol. 31*, 501−511.
11. Gläser, M., Wolff, C., and Renger, G. (1976) *Z. Naturforsch. 31C*, 712−721.
12. Renger, G., Gläser, M., and Buchwald, H. E. (1976) *Biochim. Biophys. Acta 461*, 392−402.
13. Schlodder, E., Brettel, K., and Witt, H. T. (1985) *Biochim. Biophys. Acta 808*, 123−131.
14. Van Gorkom, H. J., and Donze, M. (1973) *Photochem. Photobiol. 17*, 333−342.
15. Hoganson, C. W., and Babcock, G. T. (1997) *Science 277*, 1953−1956.
16. Hoganson, C. W., Lydakis-Simantiris, N., Tang, X. S., Tommos, C., Warncke, K., Babcock, G. T., Diner, B. A., McCracken, J., and Styring, S. (1995) *Photosynth. Res. 46*, 177−184.
17. Barry, B. A., and Babcock, G. T. (1987) *Proc. Natl. Acad. Sci. U.S.A. 84*, 7099−7103.
18. Ahlbrink, R., Haumann, M., Cherepanov, D., Bögershausen, O., Mulkidjanian, A., and Junge, W. (1998) *Biochemistry 37*, 1131−1142.
19. Schlodder, E., and Witt, H. T. (1999) *J. Biol. Chem. 274*, 30387−30392.
20. Hays, A. A., Vassiliev, I. R., Golbeck, J. H., and Debus, R. J. (1998) *Biochemistry 37*, 11352−11365.
21. Tommos, C., and Babcock, G. T. (2000) *Biochim. Biophys. Acta 1458*, 199−219.
22. Christen, G., and Renger, G. (1999) *Biochemistry 38*, 2068−2077.
23. Christen, G., Seeliger, A., and Renger, G. (1999) *Biochemistry 38*, 6082−6092.
24. Schilstra, M. J., Rappaport, F., Nugent, J. H. A., Barnett, C. J., and Klug, D. R. (1998) *Biochemistry 37*, 3974−3981.
25. Van Gorkom, H. J. (1996) *Photosynth. Res. 48*, 107−116.
26. Vos, M. H., van Gorkom, H. J., and van Leeuwen, P. J. (1991) *Biochim. Biophys. Acta 1056*, 27−39.

27. Vos, M. H., and van Gorkom, H. J. (1988) *Biochim. Biophys. Acta 934*, 293−302.
28. Robinson, H. H., and Yocum, C. F. (1980) *Biochim. Biophys. Acta 590*, 97−106.
29. Schowen, R. L. (1977) in *Isotope Effects on Enzyme-Catalyzed Reactions* (Cleland, W. W., O'Leary, M. H., and Northrop, D. B., Eds.) pp 64−99, University Park Press, Baltimore, MD.
30. Herman, J. R., Londo, T. R., Rahman, N. A., and Barisas, B. G. (1992) *Rev. Sci. Instrum. 63*, 5454−5458.
31. Straume, M., and Johnson, L. J. (1992) in *Methods in Enzymology, Volume 210: Numerical Computer Methods* (Brand, L., and Johnson, L. J., Eds.) pp 117−129, Academic Press, New York.
32. Van Gorkom, H. J. (1986) in *Light Emission by Plants and Bacteria* (Govindjee, Amesz, J., and Fork, D. C., Eds.) pp 267−289, Academic Press Inc., Orlando, FL.
33. Mathis, P., Butler, W. L., and Satoh, K. (1979) *Photochem. Photobiol. 30*, 603−614.
34. Bowes, J. M., and Crofts, A. R. (1980) *Biochim. Biophys. Acta 590*, 373−384.
35. Robinson, H. H., and Crofts, A. R. (1983) *FEBS Lett. 153*, 221−226.
36. Putrenko, I. I., Vasil'ev, S., and Bruce, D. (1999) *Biochemistry 38*, 10632−10641.
37. Renger, G., Eckert, H. J., Bergmann, A., Bernarding, J., Liu, B., Napiwotzki, A., Reifarth, F., and Eichler, H. J. (1995) *Aust. J. Plant Physiol. 22*, 167−181.
38. De Wijn, R., and van Gorkom, H. J. (1998) in *Photosynthesis: mechanisms and effects* (Garab, G., Ed.) pp 1125−1128, Kluwer Academic Publishers, Dordrecht.
39. Hemelrijk, P. W., and van Gorkom, H. J. (1996) *Photosynth. Res. 48*, 197−203.
40. Hemelrijk, P. W., and van Gorkom, H. J. (1996) *Biochim. Biophys. Acta 1274*, 31−38.
41. Arnason, T., and Sinclair, J. (1976) *Biochim. Biophys. Acta 449*, 581−586.
42. Lavergne, J., and Leci, E. (1993) *Photosynth. Res. 35*, 323−343.
43. Paillotin, G. (1976) *J. Theor. Biol. 58*, 237−252.
44. Joliot, P., and Joliot, A. (1964) *C. R. Acad. Sci. Paris 258*, 4622−4625.
45. Szabó, Z. G. (1969) in *The Theory of Kinetics* (Bamford, C. H., and Tipper, C. F. H., Eds.) pp 1−79, Elsevier Publishing Company, Amsterdam.
46. Pokorny, A., Wulf, K., and Trissl, H. W. (1994) *Biochim. Biophys. Acta 1184*, 65−70.
47. Lavergne, J., and Rappaport, F. (1998) *Biochemistry 37*, 7899−7906.
48. Rappaport, F., Porter, G., Barber, J., Klug, D. R., and Lavergne, J. (1995) in *Photosynthesis: from light to biosphere* (Mathis, P., Ed.) pp 345−348, Kluwer Academic Publishers, Dordrecht.
49. Wincencjusz, H., Yocum, C. F., and van Gorkom, H. J. (1998) *Biochemistry 37*, 8596−8604.
50. Velthuys, B. R. (1981) *FEBS Lett. 126*, 277−281.
51. Velthuys, B. R. (1982) in *Function of Quinones in Energy Conserving Systems* (Trumpower, B. L., Ed.) pp 401−408, Academic Press, New York.
52. Rich, P. R. (1981) *Biochim. Biophys. Acta 637*, 28−33.
53. Okamura, M., Paddock, M. L., Graige, M. S., and Feher, G. (2000) *Biochim. Biophys. Acta 1458*, 148−163.
54. De Grooth, B. G., van Gorkom, H. J., and Meiburg, R. F. (1980) *Biochim. Biophys. Acta 589*, 299−314.
55. Meiburg, R. F., van Gorkom, H. J., and van Dorssen, R. J. (1983) *Biochim. Biophys. Acta 724*, 352−358.
56. Mamedov, M. D., Beshta, O. E., Gurovskaya, K. N., Mamedova, A. A., Neverov, K. D., Samuilov, V. D., and Semenov, A. Yu. (1999) *Biochemistry (Moscow) 64*, 504−509.
57. Dekker, J. P., Plijter, J. J., Ouwehand, L., and van Gorkom, H. J. (1984) *Biochim. Biophys. Acta 767*, 176−179.
58. Rappaport, F., Blanchard-Desce, M., and Lavergne, J. (1994) *Biochim. Biophys. Acta 1184*, 178−192.
59. Lydakis-Simantiris, N., Ghanotakis, D. F., and Babcock, G. T. (1997) *Biochim. Biophys. Acta 1322*, 129−140.
60. Bögershausen, O., Haumann, M., and Junge, W. (1996) *Ber. Bunsen-Ges. Phys. Chem. 100*, 1987−1992.
61. Karge, M., Irrgang, K. D., and Renger, G. (1997) *Biochemistry 36*, 8904−8913.
62. Arnason, T., and Sinclair, J. (1976) *Biochim. Biophys. Acta 1976*, 517−523.

BI002824Z